Proc. Natl. Acad. Sci. USA
Vol. 91, pp. 12482–12486, December 1994
Biochemistry

Crystal structure of fructose-1,6-bisphosphatase complexed with fructose 2,6-bisphosphate, AMP, and Zn^{2+} at 2.0-Å resolution: Aspects of synergism between inhibitors

YAFENG XUE, SHENGHUA HUANG, JIIN-YUN LIANG, YIPING ZHANG*, AND WILLIAM N. LIPSCOMB†

Gibbs Chemical Laboratory, Harvard University, 12 Oxford Street, Cambridge, MA 02138

Contributed by William N. Lipscomb, September 19, 1994

ABSTRACT **The crystal structure of fructose-1,6-bisphosphatase (Fru-1,6-Pase; EC 3.1.3.11) complexed with Zn^{2+} and two allosteric regulators, AMP and fructose 2,6-bisphosphate (Fru-2,6-P_2) has been determined at 2.0-Å resolution. In the refined model, the crystallographic *R* factor is 0.189 with rms deviations of 0.014 Å and 2.8° from ideal geometries for bond lengths and bond angles, respectively. A 15° rotation is observed between the upper dimer C1C2 and the lower dimer C3C4 relative to the R-form structure (fructose 6-phosphate complex), consistent with that expected from a T-form structure. The major difference between the structure of the previously determined Fru-2,6-P_2 complex (R form) and that of the current quaternary T-form complex lies in the active site domain. A zinc binding site distinct from the three binding sites established earlier was identified within each monomer. Helix H4 (residues 123–127) was found to be better defined than in previously studied ligated Fru-1,6-Pase structures. Interactions between monomers in the active site domain were found involving H4 residues from one monomer and residues Tyr-258 and Arg-243 from the adjacent monomer. Cooperativity between AMP and Fru-2,6-P_2 in signal transmission probably involves the following features: an AMP site, the adjacent B3 strand (residues 113–118), the metal site, the immediate active site, the short helix H4 (residues 123–127), and Tyr-258 and Arg-243 from the adjacent monomer within the upper (or lower) dimer. The closest distance between the immediate active site and that on the adjacent monomer is only 5 Å. Thus, the involvement of H4 in signal transmission adds another important pathway to the scheme of the allosteric mechanism of Fru-1,6-Pase.**

Fructose-1,6-bisphosphatase (Fru-1,6-Pase, EC 3.1.3.11) catalyzes the hydrolysis of D-fructose 1,6-bisphosphate to D-fructose 6-phosphate (Fru-6-*P*) and inorganic phosphate (1, 2). Divalent metal ions, such as Mg^{2+}, Mn^{2+}, Co^{2+}, or Zn^{2+}, are required for catalytic activity (1, 3).

As a key enzyme in the gluconeogenesis pathway, Fru-1,6-Pase is regulated by two inhibitors: AMP and fructose 2,6-bisphosphate (Fru-2,6-P_2) (2, 4–7). Both AMP and Fru-2,6-P_2 also act as strong activators for phosphofrucokinase, a major regulatory enzyme in the opposing glycolytic pathway. Normally, there is a relatively stable AMP pool under *in vivo* conditions. In contrast, the Fru-2,6-P_2 concentration, which signals the level of glucagon (inversely) and glucose (proportionally), is subject to a wide range of fluctuation (8). Therefore, the modulation by Fru-2,6-P_2 is ordinarily more physiologically relevant to the coordinated control of the two reciprocal processes, glycolysis and glyconeogenesis. In addition, synergistic interaction is observed for inhibition by AMP and Fru-2,6-P_2 (4, 7, 9). Plausible mechanisms for this synergistic interaction between AMP and Fru-2,6-P_2 have recently been considered (10, 11).

Pig kidney Fru-1,6-Pase is a tetramer having D_2 symmetry. Each of the four monomers has 335 amino acids. Crystallographic studies of complexes of Fru-1,6-Pase established two quaternary conformations, the R and the T forms, which differ by a 17° rotation of the lower dimer C3C4 relative to the upper dimer C1C2 (12–14). The R-form structures include Fru-1,6-Pase complexed with Fru-6-*P* (2.1-Å resolution) (15), Fru-2,6-P_2 (2.6-Å resolution) (11), fructose 1,6-bisphosphate (2.5-Å resolution), 2,5-anhydroglucitol 1,6-bisphosphate (AhG-1,6-P_2, 2.6- to 3.0-Å resolution), and 2,5-anhydromannitol 1,6-bisphosphate (2.6- to 3.0-Å resolution) (16). The T-form structures include the AMP complex (2.5-Å resolution) (17) and the Fru-6-*P*–AMP–Mg complex (2.5-Å resolution) (12).

Kinetic and structural results show that binding of AMP alone at an allosteric site is sufficient to lock the enzyme into the T form. However, binding of inhibitors, such as Fru-6-*P* and Fru-2,6-P_2, to the active site in the R form does not change the quaternary structure to the T form.

By using the refined structure of Fru-1,6-Pase complexed with Fru-2,6-P_2, AMP, and Zn^{2+}‡ that we report here, we make comparisons with other structures of ligated Fru-1,6-Pase. We show that the helix H4 (residues 123–127) becomes more ordered in this Fru-2,6-P_2, AMP, and Zn^{2+} complex, and we provide a pathway from this helix to the active site, the adjacent monomer, and the AMP site via B3 strand of β-structure. The interactions involving residues in H4 probably contribute to the synergistic inhibition between AMP and Fru-2,6-P_2 and to the observed positive cooperativity of substrate binding when Fru-2,6-P_2 binds (4, 7).

METHODS

Pig kidney Fru-1,6-Pase was purified as described (12–14). Crystals of the enzyme complexed with AMP, Fru-2,6-P_2, and Zn^{2+} were obtained by dialyzing protein at 15–17 mg/ml against 20 mM Tris·HCl/1.0 mM AMP/0.2 mM Fru-2,6-P_2/6 μM $ZnCl_2$/5 mM NaN_3/1 mM 2-mercaptoethanol/0.1 mM EDTA/15% (wt/vol) polyethylene glycol (mean molecular weight, 3350) at pH 7.4 and 20°C. Crystals having a typical size of 0.8 × 0.8 × 1.2 mm^3 were obtained after 1 week of dialysis. Before being mounted for data collection, the crystals were soaked in the crystallization solution, which was changed six times during 35 h at 4°C. The Fru-2,6-P_2 was freshly made before each change of the soaking solution to

The publication costs of this article were defrayed in part by page charge payment. This article must therefore be hereby marked "*advertisement*" in accordance with 18 U.S.C. §1734 solely to indicate this fact.

Abbreviations: Fru-1,6-Pase, fructose-1,6-bisphosphatase; Fru-2,6-P_2, fructose 2,6-bisphosphate; Fru-6-*P*, fructose 6-phosphate; AhG-1,6-P_2, 2,S-anhydroglucitol 1,6-bisphosphate.

*Present address: Syntex Discovery Research, 3401 Hillview Avenue, Palo Alto, CA 94303.
†To whom reprint requests should be addressed.

‡The atomic coordinates and structure factors have been deposited in the Protein Data Bank, Chemistry Department, Brookhaven National Laboratory, Upton, NY 11973 (reference 1FRP).

minimize possible hydrolysis of the 2-phosphate of Fru-2,6-P_2.

The diffraction data were collected using the *R*-axis image plate area detector on a Rigaku (Danvers, MA) rotating anode generator operating at 5.4 kW at Hengming Ke's laboratory (University of North Carolina). A total of 115,147 reflections was collected and reduced to 49,540 symmetry-independent reflections. The data are 82.8% complete to 2.0-Å resolution with an R_{merge} value of 0.0744.

The starting model for the refinement is the structure of pig kidney Fru-1,6-Pase complexed with Fru-6-*P*, AMP, and Mg^{2+} at 2.5-Å resolution (12). The ligands Fru-2,6-P_2 and AMP were included in the model based on the F_o–F_c map (contoured at 3σ). The zinc position was identified based on the F_o–F_c map (contoured at 3σ) and on criteria that include more than three contacts within 2.5 Å and reasonable angular geometry. All solvent molecules were deleted from the model before refinement. Electron density maps were calculated using the program suite CCP4 (18). Inspection of the electron density maps and manual intervention of the model were carried out using the program O (19) on an Evans and Sutherland (Salt Lake City) ESV graphics station. The structure was refined using the program X-PLOR (20). Solvent molecules were added to the model based on the following criteria: (*i*) visible density in both $2F_o$–F_c (1σ) and F_o–F_c (3σ) maps and (*ii*) contacts <3.3 Å with potential hydrogen bonding atoms. Those solvent molecules that had B values >55 Å^2 after one round of refinement were deleted before the next round of refinement. The refinement was completed at an *R* value of 0.189, and the rms deviations are 0.014 Å and 2.8° from ideal geometries for bond lengths and bond angles, respectively. The 2536 protein main-chain atoms have an rms distance of 0.36 Å between the starting model and final model. The final model contains 320 of 335 residues for each monomer and 239 water molecules in a dimer. There are two AMP and two Fru-2,6-P_2 molecules and two zinc atoms in a dimer. Analysis using the program PROCHECK (21) indicates that the overall stereochemical quality of the structure compares favorably with other well-refined structures at 2.0-Å resolution. The Ramachandran plot showed 90.2% of the nonglycine residues in "most favored regions." An estimate of 0.25 Å for the error in coordinates was made using Luzzati's method (22). In the comparison of this structure with other Fru-1,6-Pase structures, the following regions of the AMP domain (residues 9–200) and the active site domain (residues 201–335) were excluded because of poor electron density: residues 9–11, 54–71, 231–238, 267–272, and 331–335. This comparison also includes some uncertainty because the various structures were determined to resolution limits that vary from 2.0 Å for the present structure to limits of 2.1–3.0 Å for the previously determined structures (12–17).

Table 1. Statistics of x-ray data and refinement

Parameter	Value
Resolution range, Å	2.0–15.0
Total reflections, no.	115,147
Unique reflections, no.	49,540
Completeness of data, %	82.8
R_{merge}	0.074
Refinement *R* factor	0.189
rms of bond lengths, Å	0.014
rms of bond angles, degrees	2.8
B value of AMP(1)	25.5
B value of AMP(2)	26.8
B value of F-2,6-P_2(1)	23.3
B value of F-2,6-P_2(2)	24.4

The rms values are rms deviations from the ideal geometries of bond lengths and bond angles; *B* values are averaged over all nonhydrogen atoms of the ligand molecules.

Table 2. Close contacts (potential hydrogen bonds) of AMP

Ligand atom	Protein atom	Distance, Å	
		Monomer C1	Monomer C2
N1	Gln-20 Cβ	3.26	3.14
N6	Val-17 O	3.08	2.78
	Thr-31 Oγ1	2.99	3.13
O2′	Arg-140 Nη1	3.27	3.94
O3′	Tyr-113 Oη	2.72	2.67
	Arg-140 Nϵ	3.20	4.24
	Arg-140	2.86 (Nη1)	2.92 (Nη2)
OR	Glu-29 N	2.79	2.86
	Met-30 N	2.84	2.82
OL	Thr-27 N	2.76	2.78
	Thr-27 Oγ1	2.67	2.73
O′	Lys-112 Nζ	2.78	2.51
	Tyr-113 Oη	2.74	2.75

Close contacts are distances <3.30 Å and are listed for monomer C1. The corresponding distances in monomer C2 are shown without limitation on values. Arg-140 is close to the surface of the protein. The *B* values for the side chain of Arg-140 are 45 Å^2 and 52 Å^2 in monomers C1 and C2, respectively.

RESULTS AND DISCUSSION

Well-defined electron densities for Fru-2,6-P_2, AMP, and zinc ion were observed in the F_o–F_c difference map (contoured at 4σ) before adding these ligands to the model. Reasonable *B* values for these ligands were found after refinement (Table 1). Distances between the inhibitors AMP and Fru-2,6-P_2 and protein atoms are recorded in Table 2–5.

The overall structure is the T-form of the enzyme. Comparison of this structure with the R-form Fru-6-*P* complex shows a rotation between the upper dimer C1C2 and the lower dimer C3C4 of ≈15°. There is no significant structural asymmetry between monomers C1 and C2. Superposition of these two monomers (Cα atoms) yields rms fits of 0.175 Å and 0.199 Å for the active site domain and the AMP domain, respectively (Tables 2–5). The electron density and the refined binding positions of Fru-2,6-P_2 and AMP in monomer C1 are almost indistinguishable from those in monomer C2.

Superposition of the structure of the quaternary complex onto that of the AMP complex (T form, 2.5-Å resolution) yields an rms fit of the Cα atoms in the AMP domain and the active site domain of 0.394 Å (0.395 Å for C2) and 0.219 Å (0.208 Å for C2), respectively. The position of the bound AMP is essentially the same in these two structures. The largest displacements of AMP atoms are ≈0.3 Å (atom N6) and 0.7 Å (atom C5′) for the two sites, respectively. Fur-

Table 3. Close contacts (van der Waals) of AMP

Ligand atom	Protein atom	Distance, Å	
		Monomer C1	Monomer C2
C2	Met-177 Sδ	3.61	3.55
	Met-177 Cϵ	3.82	4.01
	Glu-20 Cβ	3.91	3.85
C4	Ala-24 Cβ	3.92	4.02
C5	Gly-21 Cα	3.50	3.31
C6	Gly-21 Cα	3.50	3.46
C8	Met-30 Cβ	3.69	3.54
N9	Ala-24 Cβ	3.66	3.73
C1′	Ala-24 Cβ	3.77	3.76
C2′	Met-30 Sδ	3.91	3.98
C3′	Met-30 Sδ	3.85	3.88
C5′	Tyr-113 Oη	3.57	3.51
O5′	Gly-26 Cα	3.47	3.51

Close contacts are distances <4.00 Å and are listed for monomer C1. The corresponding distances in monomer C2 are shown without limitation on values.

Table 4. Close contacts (potential hydrogen bonds) of Fru-2,6-P_2

Ligand atom	Protein atom	Distance, Å	
		Monomer C1	Monomer C2
O1	Zn	2.52	2.49
	Arg-276 Nη1	3.12	3.48
O3	Asp-121 Oδ1	2.54	2.65
	Met-248 N	2.97	3.00
O4	Met-248 N	3.13	3.03
O5	Lys-274 Nζ	2.93	3.05
O6	Lys-274 Nζ	2.82	2.74
O11	Ser-124 N	2.86	2.82
O12	Ser-123 N	2.74	2.77
O13	Lys-274 Nζ	2.92	2.70
O21	Asn-212 Nδ2	2.85	2.93
	Tyr-244 Oη	2.73	2.75
O22	Arg-243 Nη1	2.85	2.76
O23	Tyr-215 Oη	2.79	2.75
	Tyr-264 Oη	2.74	2.91

Close contacts are distances <3.30 Å and are listed for monomer C1. The corresponding distances in monomer C2 are shown without limitation on values.

Table 5. Close contacts (van der Waals) of Fru-2,6-P_2

Ligand atom	Protein atom	Distance, Å	
		Monomer C1	Monomer C2
C1	Leu-275 Cδ2	3.91	4.11
C2	Leu-275 Cδ2	3.98	4.19
C3	Met-248 Cβ	3.94	3.98
	Leu-275 Cδ2	3.84	4.00
C5	Leu-275 Cδ2	3.86	4.05

Close contacts are distances <4.00 Å and are listed for monomer C1. The corresponding distances in monomer C2 are shown without limitation on values.

thermore, corresponding Cα atoms of residues nearest AMP differ at most by ≈0.5 Å for both sites in these two structures. One region, assigned as the helix H4 (residues 123–127), was found to be better defined in the quaternary complex than in the AMP complex based on the substantially lowered *B* values (20–30 Å^2 vs. 40–50 Å^2, respectively). The interface interactions between monomers C1 and C3 and between C1 and C2 are essentially the same as in the AMP complex except those involving H4 residues in the C1C2 interface (see below).

Superposition of the quaternary structure onto the structure of the Fru-2,6-P_2 complex (R form, 2.6-Å resolution) yields an rms fit of the Cα atoms in the AMP domain and the active site domain of 1.215 Å (1.265 Å for C2) and 0.268 Å (0.267 Å for C2), respectively. Fru-2,6-P_2 binds to the enzyme in the same manner in these two structures (Fig. 1). Here again, the *B* values for helix H4 are found to be much lower in the quaternary (T form) complex than in the binary (R form) Fru-2,6-P_2 complex, indicative of a more ordered region in the quaternary complex. In addition, the Cα atoms of residues 123–127 have moved between 1.0 and 2.5 Å, giving a somewhat tightened active site cavity in the T form (Fig. 1). The T and R forms showed different interactions between the 2-phosphate oxygens of Fru-2,6-P_2 and Ser-124 of H4; in the structure of the R-form Fru-2,6-P_2 complex, one oxygen of the 2-phosphate is hydrogen-bonded to the Oγ of Ser-124 (distance, 2.94 Å), whereas in the T-form structure, oxygens of the 2-phosphate are in contact with the amide nitrogens of Ser-124 (distance, 2.86 Å) and Ser-123 (distance, 2.74 Å). The Oγ of Ser-124 is now hydrogen-bonded to the Nη1 of Arg-243 from the adjacent monomer (distance, 3.15 Å). Another significant change is the side-chain orientation of Tyr-258 from the adjacent monomer (Fig. 1). In the R-form Fru-2,6-P_2 complex, the phenol group of this Tyr is pointing to the surface of the protein, nearly parallel to the axis of H4. In the quaternary complex the side chain of Tyr-258 has rotated around Cα–Cβ >90° relative to the previous orientation in the Fru-2,6-P_2 complex and, therefore, points toward helix H4. The Oη group of Tyr-258 is hydrogen-bonded to the backbone carbonyl of Ser-124 (O) and amide of Cys-128 (N) (distances, 2.80 Å and 2.71 Å, respectively). These interactions involving Tyr-258 and Arg-243 are not present in the monomer interface in the other known T-form structures. In fact, the orientations of the side chain of Tyr-258 in other ligated structures resemble the orientation in the structure of the R-form Fru-2,6-P_2 complex. The orientation of the side chain of Tyr-258 found here in the quaternary T-form structure is seen only in the unligated R-form structure (3.0-Å resolution) in which the Oη of Tyr-258 is hydrogen-bonded to the carboxylate group of Asp-127 of the adjacent monomer (distance, 2.80 Å).

Only one zinc (*B* value, 50 Å^2) was found for each monomer of the quaternary structure (Fig. 2), and it is in the active site. This zinc is penta-coordinated with three protein ligands: Oδ2 of Asp-118, Oδ1 of Asp-121, and Oε2 of Glu-280. The O1 oxygen of Fru-2,6-P_2 is also a coordination ligand (Zn–O distance, 2.52 Å). Finally, the fifth ligand is a water molecule, 2.47 Å from zinc. The geometry of the coordination may be described as distorted tetrahedral plus the water as an extra ligand (the Fru-2,6-P_2 O1–Zn–water angle is ≈60°).

In the structure of Fru-1,6-Pase complexed with AhG-1,6-P_2 and zinc (3.0-Å resolution) (16), two zinc ions (*B* values, 70–80 Å^2) were found in the active site per monomer. One zinc is directly bonded to a 1-phosphate oxygen from the substrate analogue AhG-1,6-P_2 and is 3.5 Å from the carbox-

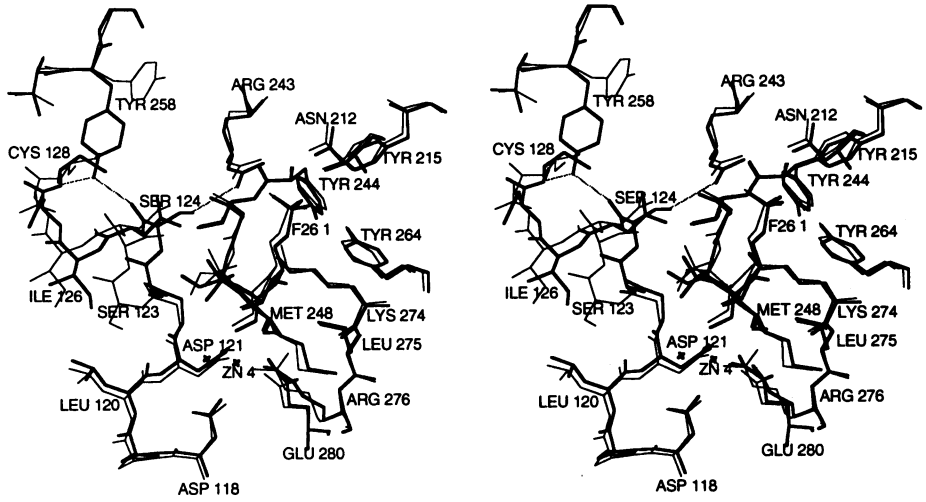

FIG. 1. Stereo picture showing active site residues. Structures of the quaternary Fru-2,6-P_2, AMP, and Zn^{2+} complex (heavy lines) and binary Fru-2,6-P_2 complex (light lines) are superimposed. The zinc position is indicated as a cross labeled ZN 4. The unlabeled × represents the ligand water. Residues Tyr-258 and Arg-243 are from the adjacent monomer. Interactions involving these two residues over the monomer interface are indicated as dashed lines. Note that helix H4 (residues 123–127) has a significant movement upon binding of AMP and Zn^{2+}. This short helix may play an important part in the communication between AMP site and the active site and communication between two adjacent monomers C1 and C2.

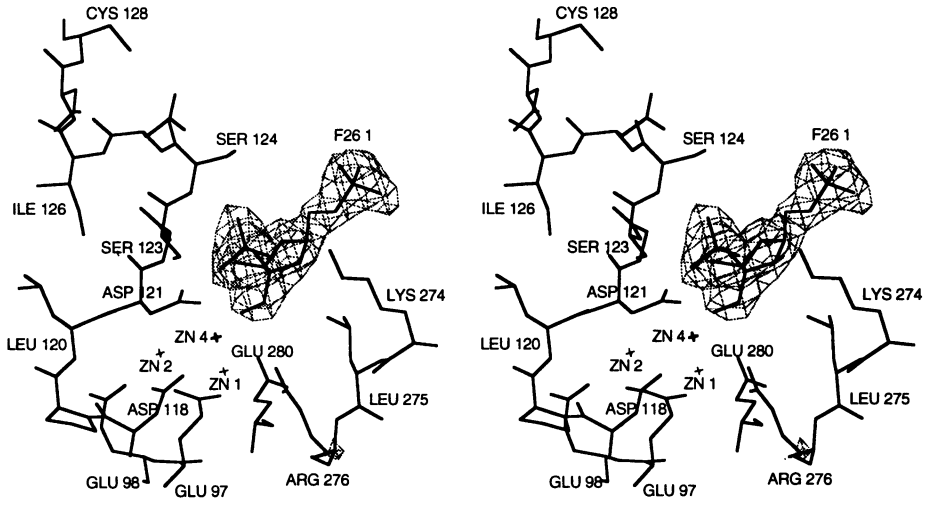

FIG. 2. Stereo picture showing the metal binding area in the active site of Fru-1,6-Pase. The bound Fru-2,6-P_2 is labeled F26 1. The electron density for the inhibitor is shown in dashed lines ($F_o - F_c$ omit map, contoured at 3σ). The boldface × (labeled ZN 4) shows the zinc position in the quaternary Fru-2,6-P_2, AMP, and Zn^{2+} complex. The two lightface ×s are positions for the two zinc ions in the AhG-1,6-P_2 complex (16) that was superimposed onto the structure of the quaternary complex. Zn 1 and Zn 2 represent binding site 1 and site 2, respectively, as previously assigned. Site 1 is coordinated to the carboxylate groups of Glu-97, Asp-118, and Glu-280 and the 1-phosphate group of substrate analogue, while site 2 is coordinated to the carboxylate groups of Glu-97 and Asp-118, the 1-phosphate group of substrate analogue, and the carbonyl oxygen of Leu-120. A third metal binding site was found in this region in the absence of substrate/substrate analogue (10). Site 3 (data not shown) for metal binding involves Glu-97, Glu-98, and Asp-118. The zinc position in the quaternary complex (site 4) is 2 Å from site 1.

ylate oxygen of Asp-121. This zinc has four ligands in approximate tetrahedral geometry. The three protein ligands are carboxylate oxygen atoms from Glu-97, Asp-118, and Glu-280. This site is known as the site 1 for metal binding in the active site. The second zinc (in site 2) in the AhG-1,6-P_2 complex is bound to Glu-97, Asp-118, Leu-120, and the 1-phosphate of the substrate analogue. In the absence of substrate or substrate analogues, zinc occurs at sites 1 and 3 (distinct from site 2). At site 3, zinc is bonded to Glu-97, Glu-98, and Asp-118, and, at a longer distance, to Asp-74 (11).

The zinc position in Fru-2,6-P_2–AMP–Zn complex (site 4) is different from the three metal sites described in the preceding paragraph. It is shifted ≈2 Å from the site 1 position in the AhG-1,6-P_2–Zn complex (Fig. 2), probably to accommodate the substitution of the 1-phosphate with 2-phosphate. This substitution exposes the O1 oxygen and provides a way for Asp-121 to interact with the metal. In the absence of metal, as illustrated in the structure of the Fru-2,6-P_2 complex, Asp-121 interacts with the inhibitor through hydrogen bonds between its carboxylate oxygens and O1 and O3 from the inhibitor. In the structure of the

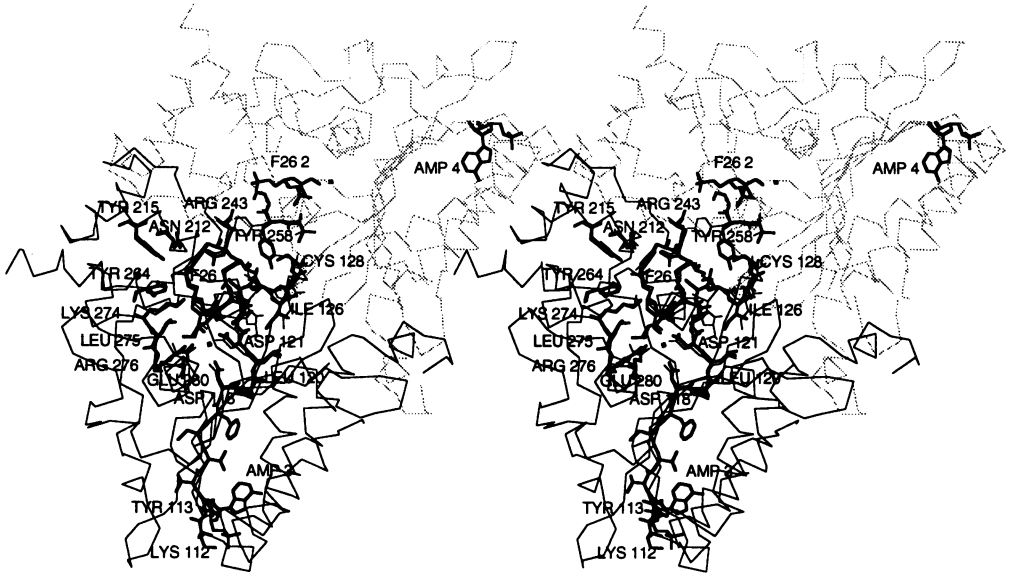

FIG. 3. Stereo picture showing the possible pathway between the AMP site and the active site. The twofold molecular axis is ≈45° off the horizontal line from the upper left corner and is in the plane of the paper. The bound Fru-2,6-P_2 (labeled F26 1) is just above the × that indicates the zinc ion. The thin lines and the dashed lines in the background are Cα traces of monomers C1 and C2, respectively. The communication between the AMP site and active site in the same monomer may go through strand B3 (residues 113–118), the metal binding area (residues 97–98, 118–121, and 280), and helix H4 (residues 123–127). Interactions involving Arg-243 and Tyr-258 provide an important pathway for signaling between C1 and C2. This pathway may be relevant to the cooperativity of metal binding and for synergism with Zn–AMP inhibition. In addition, tightening of this pathway may also explain the effect in which the substrate saturation curve changes from hyperbolic to sigmoidal upon binding of Fru-2,6-P_2 (4). The above mentioned communication within one monomer and across the dimer may, therefore, account for the synergistic inhibition of Fru-2,6-P_2 and AMP.

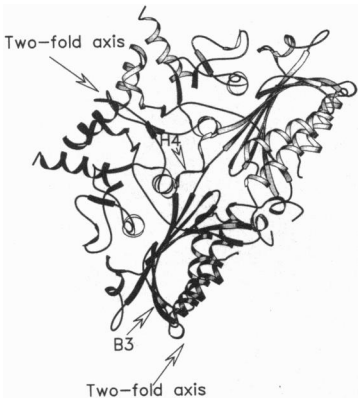

FIG. 4. Ribbon drawing of Fru-1,6-Pase dimer (half of the molecule). Only strand B3 and helix H4 are labeled. Two molecular axes (twofold) are shown. The one in the upper left relates monomer C1 (darker gray) and monomer C2 (lighter gray). The lower one generates the other half of the molecule (data not shown). This figure is comparable to Fig. 3.

Fru-2,6-P_2 complex, Asp-121 interacts with helix H7 (residues 247–258) by a van der Waals contact between its Oδ2 and the Cγ2 of Val-249 (3.5 Å). This is also the case in the AhG-1,6-P_2–Zn complex.

In the presence of both zinc and the inhibitor, as in the structure of the Fru-2,6-P_2–AMP–Zn complex, significant changes occur around Asp-121. Aside from the direct interaction with zinc (2.37 Å), its Oδ2 is now hydrogen-bonded to the amide nitrogen of Val-249 (distance, 2.87 Å) and its Oδ1 is hydrogen-bonded to the O3 of the Fru-2,6-P_2 (distance, 2.54 Å). These interactions seem to be relevant to the "cooling down" of the H4 helix and the formation of additional interactions in the monomer interface including those involving Tyr-258 and Arg-243.

The results here indicate that synergistic interaction between AMP and Fru-2,6-P_2 may be attributed to the communication between these two inhibitors in one monomer or over two monomers (Figs. 3 and 4). It becomes clear that strand B3 (residues 113–118) is part of the signaling pathway between the AMP domain and the active site domain. In addition, helix H4 is an important element in this signaling mechanism. Without binding of AMP to the enzyme, H4 is still mobile and the active site cavity is in an open mode even upon binding of Fru-2,6-P_2. The cooperativity of AMP inhibition may be achieved through signal transmission along B3, the metal binding area, first active site/H4, Tyr-258/Arg-243 from the adjacent monomer, and then to the other active site (Figs. 3 and 4). Thus, H4 is important in communication between the AMP domain and the active site domain.

The presence of zinc may be critical to effective communication. The fact that metal binding primarily involves residues from B3 provides evidence for the synergistic interactions between zinc (at high concentration) and AMP. In the current quanternary structure, zinc may contribute to the enhanced ordering of H4 and subsequently to the contraction of the active site cavity and to the additional interactions between two monomers in the active site domain.

The various zinc binding sites in this and previous studies (12–17) from this laboratory indicate that this carboxylate-rich area is an ideal place for anchoring metal ions. All of the metal ions bound to this area have high temperature factors (>40 Å) in known Fru-1,6-Pase structures. Binding of metal ions to different sites in this area not only determine the function of the metal ion but also affect the flexibility or orientation preference of H4. Furthermore, binding of metal ions to more than two specific sites or to adjacent sites may interfere with substrate binding.

Previous hypothesis for the allosteric signaling pathways of Fru-1,6-Pase primarily includes monomer interfaces in the AMP domain (23). The observation of the involvement of helix H4 in signal communication to the active site and between monomers C1 and C2 is of significance because it provides a pathway for allosteric signaling. This pathway probably contributes to the synergistic inhibition between AMP and Fru-2,6-P_2 and to the change of substrate saturation curve from hyperbolic to sigmoidal when Fru-2,6-P_2 binds to the enzyme (4, 7).

We thank Dr. H. Ke for help in data collection. This research is supported by National Institutes of Health Grant GM06920.

1. Benkovic, S. J. & deMaine, M. M. (1982) *Adv. Enzymol.* **53,** 45–82.
2. Tejwani, G. A. (1983) *Adv. Enzymol.* **54,** 121–194.
3. Gomori, G. (1943) *J. Biol. Chem.* **148,** 139–149.
4. van Schaftingen, E. & Hers, H.-G. (1981) *Proc. Natl. Acad. Sci. USA* **78,** 2861–2863.
5. van Schaftingen, E. (1987) *Adv. Enzymol. Relat. Areas Mol. Biol.* **59,** 315–395.
6. Marcus, F. (1981) in *The Regulation of Carbohydrate Formation and Utilization in Mammals*, ed. Veneziale, C. M. (University Park Press, Baltimore), pp. 269–290.
7. Pilkis, S. J., El-Maghrabi, M. R., Pilkis, J. & Claus, T. (1981) *J. Biol. Chem.* **256,** 3619–3622.
8. Schimassck, H. & Mitzkat, H. J. (1963) *Biochem. Z.* **337,** 510–518.
9. Francois, J., van Schaftingen, E. & Hers, H.-G. (1983) *Eur. J. Biochem.* **134,** 169–273.
10. Liang, J.-Y., Zhang, Y., Huang, S., Ke, H. & Lipscomb, W. N. (1992) *Proceedings of the Robert A. Welch Foundation Conference on Chemical Research*, Regulation of Proteins by Ligands (Robert A. Welch Found., Houston), Vol. 36, pp. 57–99.
11. Liang, J.-Y., Huang, S., Zhang, Y. & Lipscomb, W. N. (1992) *Proc. Natl. Acad. Sci. USA* **89,** 2404–2408.
12. Ke, H., Zhang, Y. & Lipscomb, W. N. (1990) *Proc. Natl. Acad. Sci. USA* **87,** 5243–5247.
13. Ke, H., Thorpe, C. M., Seaton, B. A., Lipscomb, W. N. & Marcus, F. (1990) *J. Mol. Biol.* **212,** 513–539.
14. Ke, H., Thorpe, C. M., Seaton, B. A., Lipscomb, W. N. & Marcus, F. (1990) *J. Mol. Biol.* **214,** 950.
15. Ke, H., Zhang, Y., Liang, J. & Lipscomb, W. N. (1991) *Proc. Natl. Acad. Sci. USA* **88,** 2989–2993.
16. Zhang, Y., Liang, J.-Y., Huang, S., Ke, H. & Lipscomb, W. N. (1993) *Biochemistry* **32,** 1844–1857.
17. Ke, H., Liang, J., Zhang, Y. & Lipscomb, W. N. (1991) *Biochemistry* **30,** 4412–4420.
18. Bailey, S. (1994) *Acta Crystallogr. D* **50,** 760–763.
19. Jones, T. A., Zou, J.-Y., Cowan, S. W. & Kjeldgaard, M. (1991) *Acta Crystallogr. A* **47,** 110–119.
20. Brünger, A. T., Kuriyan, J. & Karplus, M. (1987) *Science* **235,** 458–460.
21. Laskowski, R. A., MacArthur, M. W., Moss, D. S. & Thornton, J. M. (1993) *J. Appl. Crystallogr.* **26,** 283–291.
22. Luzzati, V. (1952) *Acta Crystallogr. A* **5,** 801–810.
23. Zhang, Y., Liang, J.-Y., Huang, S. & Lipscomb, W. N. (1994) *J. Mol. Biol.*, in press.